Journal of Molecular Spectroscopy 405 (2024) 111948

Contents lists available at ScienceDirect

Journal of Molecular Spectroscopy

journal homepage: www.elsevier.com/locate/yjmsp

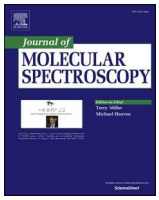

# Geometry of the argon…imidazole complex revealed by the microwave spectra of four isotopologues

Ryan Welch [a,1], Mark D. Marshall [a,*], Eva Gougoula [b,2], Nicholas R. Walker [b,*], Helen O. Leung [a,*]

[a] Department of Chemistry, Amherst College, P. O. Box 5000, Amherst, MA 01002-5000, USA
[b] Chemistry-School of Natural and Environmental Sciences, Newcastle University, Bedson Building, Newcastle-upon-Tyne, UK

ARTICLE INFO

*Keywords:*
Intermolecular interactions
Microwave spectroscopy
Rotational spectroscopy
Molecular structure

ABSTRACT

The rotational spectra of four isotopologues of an isolated complex formed between an argon atom and imidazole, Ar…imidazole, have been recorded in the 6–19 GHz region by Fourier transform microwave spectroscopy. Rotational transition frequencies have been fitted to Watson's *S*-reduced Hamiltonian to yield rotational, centrifugal distortion and nuclear quadrupole coupling constants for the complex. Rotational constants determined for the parent and three $^{15}$N-containing isotopologues allow the three-dimensional structure of the complex to be described. The two angles, θ and ϕ, which define the orientation of the Ar atom relative to the imidazole ring have been determined for the first time in addition to the distance between Ar and the center of mass of the imidazole sub-unit, *R*. Fitting of structural parameters to the experimentally-determined moments of inertia yields a structure where Ar is positioned above the ring plane at a distance of 3.519 Å from the center of mass of the imidazole sub-unit. In the experimentally determined, average geometry, the intermolecular axis (drawn through Ar and the center of mass of the imidazole sub-unit) is oriented at 6° from the normal to the ring plane. The experimental results allow for four alternative possibilities for ϕ with 62.0(39)° being that which is most consistent with expectations for this parameter based on previous work. The experimentally-determined nuclear quadrupole coupling constants imply that the electric field gradient at each of the nitrogen nuclei of imidazole does not significantly change on formation of the complex with Ar.

## 1. Introduction

Imidazole, a planar aromatic heterocycle, contains three functionalities: a π electron cloud, a hydrogen bond donor (a pyrrolic nitrogen, N1), and a hydrogen bond acceptor (a pyridinic nitrogen, N3). Extensive hydrogen bonding is found in both its solid and liquid phases leading to high melting (90°C) and boiling (256°C) points [1]. It is a key component of the nucleic acid bases, adenine and guanine, and of the side chain of histidine. It has an important role in biochemistry, being able to participate in multiple weak interactions simultaneously. The central objective of the present work involves characterization of the weak interaction between an imidazole molecule and an argon atom within an isolated, gas phase complex formed of these sub-units. The interaction between argon and imidazole is selected for study because it is an important, prototypical example of a dispersion interaction occurring between the π electrons of an imidazole ring and a polarizable, neutral species.

Recent studies have explored how weak interactions formed between imidazole derivatives and other molecules depend on (electronic and geometric) molecular structure and internal dynamics. The present study reports structural parameters that will serve as key benchmarks within this broader context of contemporary interest in the molecular physics of such weak interactions. For example, recent studies [2] have explored the geometries of complexes formed between $H_2O$ and each of *N*-methylimidazole and 2-methylimidazole. Detailed studies of complexes formed between an argon atom and each of *N*-methylimidazole, 2-methylimidazole, 4-methylimidazole and 5-methylimidazole are currently progressing at Newcastle University by authors of this work. Analyses of spectra of complexes which contain methylimidazole are challenging because of splittings introduced by internal rotation of the $CH_3$ group. It will not always be possible to obtain spectra for many different isotopologues, limiting the structural information that may be

* Corresponding authors.
*E-mail addresses:* mdmarshall@amherst.edu (M.D. Marshall), nick.walker@newcastle.ac.uk (N.R. Walker), hleung@amherst.edu (H.O. Leung).
[1] Present address: KieranTimberlake, 841 North American Street, Philadelphia, PA 19123, USA.
[2] Present address: Deutsches Elektronen-Synchrotron DESY, Notkestr. 85, 22607 Hamburg, Germany.

https://doi.org/10.1016/j.jms.2024.111948
Received 19 July 2024; Received in revised form 22 August 2024; Accepted 11 September 2024
Available online 23 September 2024

obtained from such studies. The present work will establish benchmark results for the Ar…imidazole complex which represents a logical starting point from which to examine dispersion interactions with an imidazole ring. The results will inform and support ongoing and future analyses of rotational spectra of complexes that contain derivatives of imidazole.

Christen et al.'s comprehensive analysis of the microwave spectrum of imidazole [3] built on previous works [4,5] to provide a complete substitution structure from information available for eleven isotopologues of the molecule. In addition to structural information, values of nuclear quadrupole coupling constants were determined for each nitrogen atom, providing insight into the electronic environment within the ring. Recently, the microwave spectrum of imidazole has been re-analyzed with the aim of providing more accurate values of transition frequencies [6]. The first rotational spectrum (measured from 60 − 78 GHz) of the isolated, gas phase complex, Ar…imidazole, was reported by Caminati *et al.* [7] and analyzed to determine the distance between Ar and the center of mass of imidazole. Nuclear quadrupole hyperfine structure was not resolved and data were recorded for only one isotopologue, precluding determination of the three-dimensional structure of this complex. We present here an analysis of low *J* rotational transitions (between 6 and 19 GHz) for four isotopologues of Ar…imidazole, which allows for the precise determination of rotational constants and nuclear quadrupole coupling constants. These results allow for a more comprehensive, three-dimensional description of the geometry of the Ar…imidazole complex than has been available previously. Furthermore, analysis of the nuclear quadrupole coupling constants of the complex will show that the attachment of Ar to imidazole is not accompanied by significant changes in electric field gradients at the nitrogen nuclei within the molecule.

## 2. Experiment

Two different microwave spectrometers are used during the present work. These employ alternative methods of sample preparation, each of which is found to generate intense signals for imidazole and the Ar…imidazole complex. A Balle-Flygare Fourier transform microwave (FTMW) spectrometer is used at Amherst College [8] to measure line centers of transition frequencies for isotopologues of Ar…imidazole in the 6–19 GHz region. Typically, 4k data points are collected during measurements performed using this instrument giving a resolution element of 2.44 kHz. For very strong signals, 8k data points are collected and these are either Fourier transformed directly or zero-filled to a 16k record length before Fourier transformation, giving a 1.22 or 0.61 kHz resolution element, respectively. The nozzle used to introduce the chemical sample into the vacuum chamber is mounted parallel to the resonator axis. As a result, each spectral line is Doppler doubled, and the mean frequency of the two Doppler components gives the rest frequency of the transition. Spectral lines of approximately 15–25 kHz FWHM are recorded such that the standard deviation achieved by fits of line center frequencies to the rotational Hamiltonian is of the order of a few kHz. The other spectrometer used by the present work is a chirped-pulse (CP) FTMW spectrometer at Newcastle University [9,10]. The broad bandwidth of this instrument allows for the simultaneous recording of many transitions from 7.5 – 18 GHz and the alignment of the nozzle axis perpendicular to the microwave propagation means recorded transitions are not Doppler doubled. However, this spectrometer has lower resolution than the Balle-Flygare FTMW spectrometer with respect to the measurement of line center frequencies. During the present work, therefore, this CP-FTMW spectrometer is used only to perform broad surveys of spectral features and not to measure individual line center frequencies.

A heated reservoir (temperature of about 100°C) is used to introduce imidazole into the argon flow using the Balle-Flygare FTMW spectrometer. The brass nozzle with reservoir, similar to the arrangement described by Suenram *et al.* [11], is constructed as shown in Fig. 1. A flexible, Kapton insulated heater wraps around the nozzle and up to 10 W of power can be applied to the heater. The heated nozzle, after being attached to a pulsed valve, is inserted into one of the mirrors that form the Fabry-Perot cavity. The nozzle and mirror are not in contact so that the only insulator between the two is vacuum, which works effectively. The resulting gaseous sample is introduced by the pulsed nozzle into the Fabry-Perot cavity of the spectrometer while employing a backing pressure of 3–4 bar. A pulse of microwave radiation is then applied to excite the species of interest. After the excitation pulse has dissipated, the molecular free induction decay (FID) signal is coupled out of the cavity, down-converted twice by a two-stage heterodyne detection system to a center frequency of 2.5 MHz, and digitized at a 10 MHz sampling frequency. The signal is corrected for background, Fourier transformed, and averaged to generate the resolution and linewidth as described in the opening paragraph of this section. Imidazole-1,3-$^{14}N_2$ is obtained from Acros (99% purity). Three $^{15}N$ substituted isotopologues are supplied (in two samples) by Icon Services: one sample of the doubly substituted imidazole-1,3-$^{15}N_2$ (99% $^{15}N$) and another comprising 25% each of two singly substituted isotopologues, imidazole-1-$^{15}N$ and imidazole-3-$^{15}N$. The rest of the mixture contains an equal amount of the most abundant isotopologue (imidazole-1,3-$^{14}N_2$) and the doubly substituted isotopologue (imidazole-1,3-$^{15}N_2$).

The spectrum displayed in Fig. 2 is recorded using the chirped-pulse FTMW spectrometer while employing laser vaporization followed by supersonic expansion for generation of the Ar…imidazole complex. A target rod is initially prepared through compression of mixed solid crystalline salts (containing isotopes in their naturally-occurring abundance ratios) of imidazole and silver iodide (AgI) using a hydraulic bench press. This rod is mounted into a bespoke mount positioned a few millimeters downstream of the pulsed nozzle used to introduce gaseous sample into the vacuum chamber of the spectrometer. A focused Nd:YAG

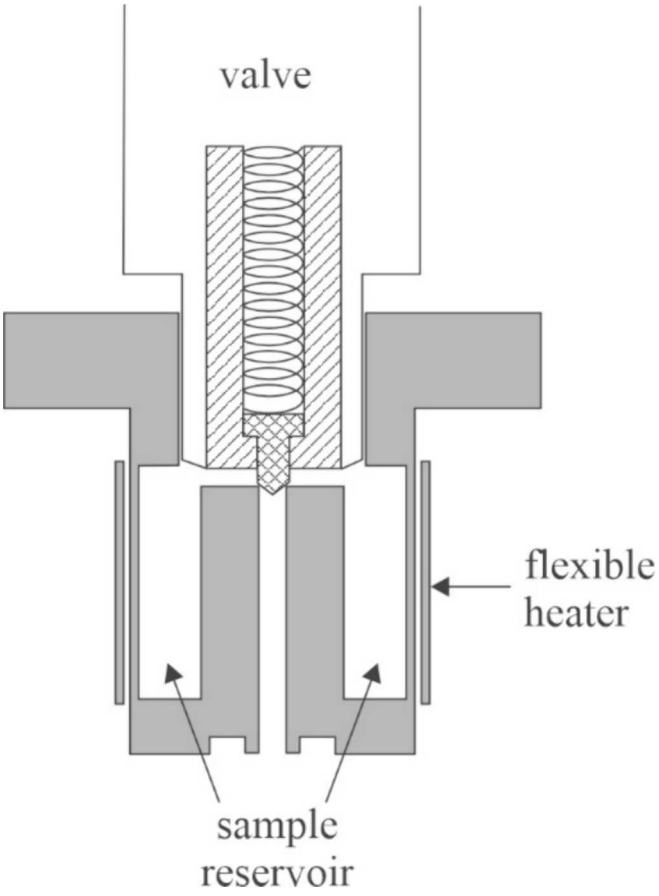


**Fig. 1.** A schematic diagram of the heated nozzle used at Amherst College for the study of Ar-imidazole.

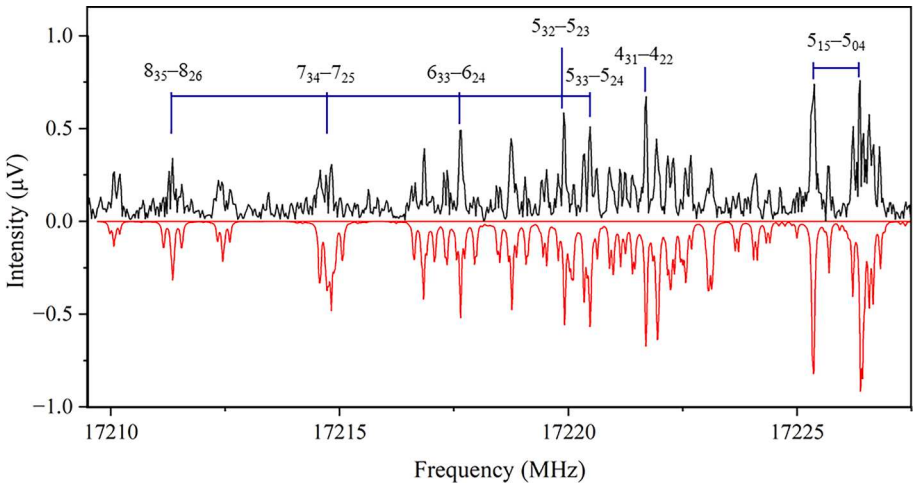


**Fig. 2.** Section of CP-FTMW spectrum. The black trace is the experimentally-recorded spectrum, obtained from an average over 240k FIDs and representing 30k gas pulse/laser vaporization shots. The red trace (displayed against an inverted scale) is simulated from the experimentally-determined spectroscopic parameters under the assumptions of a rotational temperature of 2 K and a (FWHM) linewidth of 50 kHz.

laser pulse (wavelength of 1064 nm, pulse duration of 10 ns, pulse energy of ~40 mJ) is then used to vaporize material from the surface of the rod into a flow of argon gas (backing pressure of 6 bar). The rod is continually rotated and translated during experiments. The design features of this laser vaporization source have been described in detail previously [12]. The resulting gas mixture undergoes supersonic expansion and microwave spectra are recorded for molecules and complexes within the expanding sample. Following a 1 μs chirped polarization pulse, the resulting FID is down-converted to a 0.5 – 12. GHz bandwidth and digitized at a 25 Gs $s^{-1}$ sampling rate for 20 μs. Eight polarization/digitization cycles are performed for each opening of the pulsed valve. A wide range of target rod compositions have been employed during experiments performed to study a series of imidazole-containing complexes. The results displayed in Fig. 2 are obtained while using a rod consisting of AgI and imidazole (in a 1:1 ratio by mass). This composition is found to yield transitions of acceptable signal/noise for the Ar…imidazole complex even while transitions of other molecules and complexes are also observed within the spectra.

## 3. Quantum chemical calculations

The equilibrium geometry of the Ar…imidazole complex is determined using Density Functional Theory (DFT) calculations, as implemented in the ORCA 5.0 package [13,14]. The hybrid functional of Becke-Lee-Yang-Parr (B3LYP) [15,16] is employed with Grimme's dispersion correction (D3BJ) [17,18], along with the augmented triple-ζ (aug-cc-pVTZ) [19] basis set. The optimized geometry is shown in Fig. 3. Calculated molecular parameters including rotational constants ($A_e$, $B_e$, $C_e$), nuclear quadrupole coupling constants ($\chi_{aa}, \chi_{bb}, \chi_{cc}, \chi_{ab}, \chi_{ac}, \chi_{bc}$) for each nitrogen nucleus (with signs for the off-diagonal components consistent with the right-handed coordinate system shown in Fig. 3) and the magnitudes of the electric dipole moment components ($\mu_a, \mu_b$, and $\mu_c$) are summarized in Table S1 of the supplementary information. The calculated atomic coordinates ($r_e$) are given in Table S2.

## 4. Results

### 4.1. Spectral analysis

The values of spectroscopic parameters reported by Caminati *et al.* [7] allowed for transitions of Ar…imidazole to be readily identified during the present work. Most are *b*-type with only a small number of *c*-type transitions (and none for Ar…imidazole-1-$^{15}$N) observed. This contrasts with the situation for the imidazole monomer where mainly *a*-type transitions were observed. This is expected because, as noted by Caminati *et al.*, each of the inertial axes of Ar…imidazole is significantly rotated (by almost 90°) from their orientations (relative to the positions of the atoms within the imidazole ring) in the isolated imidazole

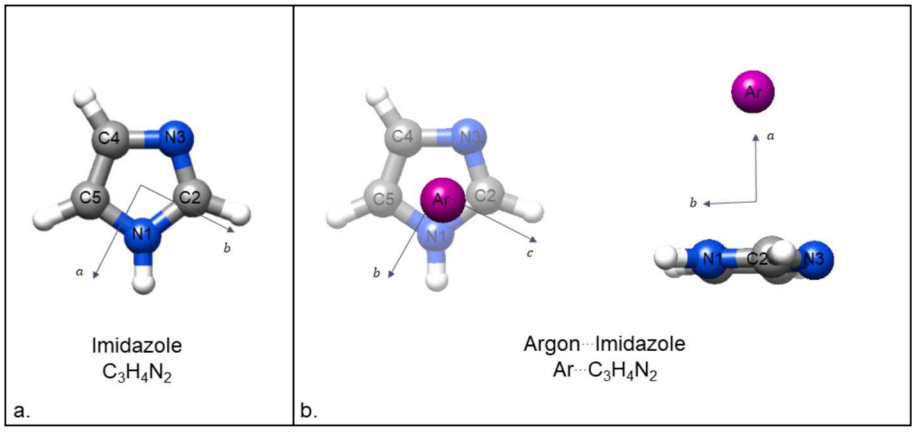


**Fig. 3.** The *a* and *b* inertial axes for the imidazole monomer (left) and for Ar…imidazole (right). The small purple sphere in the left figure of the right panel indicates the projection of argon in the imidazole plane in the complex. Atom colors: C, dark gray; H, light gray, N, blue; Ar, purple.

monomer. In the absence of nuclear quadrupole coupling interactions, the population in each rotational energy level in the doubly substituted $^{15}$N isotopologue is not divided amongst hyperfine levels; therefore, we are able to observe more rotational transitions for this isotopologue than for the most naturally-abundant isotopologue. On the other hand, since each of the singly-substituted $^{15}$N isotopologues is generated from a sample containing only 25% of the corresponding imidazole monomer, the number of rotational transitions observed is fewer even though the hyperfine structure is much simpler than that of the most abundant isotopologue.

The spectra for the $2_{12}$–$1_{01}$ transitions for all isotopologues are shown in Fig. 4. The hyperfine structure of the most abundant isotopologue and the singly-substituted isotopologues is displayed over a 4.6 MHz region for comparison. The complexity of the spectrum of the most abundant isotopologue is apparent. Conversely, the spectrum of the doubly-substituted isotopologue is very simple, showing only a Doppler doublet (this spectrum was taken before all experimental conditions were optimized; thus, it has a relatively low signal-to-noise ratio). The spectrum of each isotopologue is analyzed and fitted while using the Watson *S*-reduced Hamiltonian ($H_R$) [20] in the $I^r$ representation with the inclusion of the interaction between the electric field gradient and the nuclear quadrupole moment for each $^{14}$N nucleus. For each of the singly-substituted species, the total angular momentum is $F = J + I_{^{14}N}$, where $J$ is the rotational angular momentum of the molecule and $I_{^{14}N}$ is the spin angular moment of the $^{14}$N nucleus. For the most abundant isotopologue where two quadrupolar $^{14}$N nuclei are present, we first couple the rotational angular momentum with the spin of N3 ($I_{^{14}N3}$) to give an intermediate angular momentum $F_1$, which in turn is coupled with the spin of N1 ($I_{^{14}N1}$) to give the total angular momentum, $F$. This coupling scheme is appropriate because of the dissimilar electric field gradients experienced by the two nuclei and provides a useful labelling for the resulting hyperfine energy levels.

The spectroscopic constants are determined using Pickett's nonlinear least squares program [21] and listed in Table 1. Because of the large number of rotational transitions observed, in addition to the rotational constants, five quartic and two sextic centrifugal distortion constants are determined for Ar-imidazole-1,3-$^{15}N_2$. For the other isotopologues, some of the centrifugal distortion constants cannot be determined and are fixed to the values of those for the doubly substituted isotopologue. All diagonal components of the nuclear quadrupole coupling tensors are determined for N1 and N3. In addition, an off-diagonal component, $\chi_{bc}$, is available for N3 (See Section 4.3 for a discussion of the sign for this component). The three quartic centrifugal distortion constants, $D_J$, $D_{JK}$, and $D_K$, differ by only 1–3% among the isotopologues. As expected, the magnitudes of these constants are greatest for the lightest isotopologue, Ar-imidazole-1,3-$^{14}N_2$, and smallest for the heaviest isotopologue, Ar…imidazole-1,3-$^{15}N_2$. Contrary to this trend, the magnitude of $d_1$ for Ar…imidazole-1,3-$^{15}N_2$ is more than twice that for Ar…imidazole-1,3-$^{14}N_2$. This constant, however, is 2–3 orders of magnitude smaller than $D_J$, $D_{JK}$, and $D_K$. With the exception of Ar-imidazole-1,3-$^{15}N_2$, the centrifugal distortion constants for the other isotopologues cannot all be determined independently. As a result, it is not appropriate to compare the values of this constant nor attribute significance to the observed variations among the isotopologues. A comparison of the spectroscopic constants determined here for the most abundant isotopologue with those of Caminati *et al.* [7] shows that there is good agreement with the present study yielding the more precise values. Observed and calculated transition frequencies with assignments for all isotopologues studied are provided in Tables S3 – S6 of the supplementary information.

### 4.2. Structure determination

Ar…imidazole is a slightly asymmetric near-prolate top with an asymmetry parameter between −0.990 and −0.995 for each of the four isotopologues. To determine the structure of the complex, we take the substitution geometry of the imidazole monomer as described by Christen *et al.* [3] and assume that it remains unchanged upon

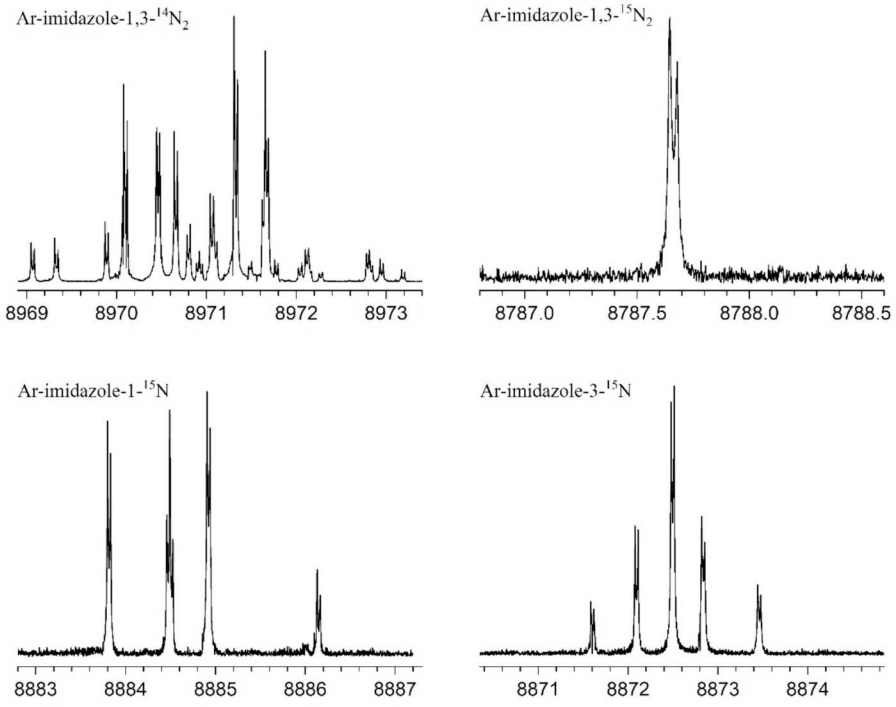


**Fig. 4.** The $2_{12}$–$1_{01}$ rotational transition for four isotopologues of Ar-imidazole. The transitions for the most abundant and singly substituted isotopologues are displayed over a 4.6 MHz range, and are obtained by concatenating the center portions of overlapping spectra, each approximately 1 MHz wide and optimized for their individual ranges. The spectral lines for the doubly substituted isotopologue comes from one single spectrum, and is shown over a 1.75 MHz range. Each spectral line is Doppler doubled. The number of averages for each 1 MHz spectrum varies, but is typically between 500 and 1000.

**Table 1**
Spectroscopic constants (in MHz, except as otherwise noted) for four isotopologues of Ar-imidazole obtained in this work[a] and by Caminati et al. [7].

| | This work | | | | Caminati *et al.*[b] |
|---|---|---|---|---|---|
| | Ar…imidazole-1,3-$^{14}N_2$ | Ar…imidazole-1-$^{15}N$ | Ar…imidazole-3-$^{15}N$ | Ar…imidazole-1,3-$^{15}N_2$ | Ar…imidazole-1,3-$^{14}N_2$ |
| $A$ | 4829.519483(63)[c] | 4771.93556(23) | 4764.99370(35) | 4707.48786(13) | 4829.51(1) |
| $B$ | 1389.270161(30)[c] | 1382.962345(39) | 1383.074836(73) | 1376.666390(34) | 1389.18(3) |
| $C$ | 1380.639372(41)[c] | 1371.029369(57) | 1369.28128(11) | 1360.159588(47) | 1380.83(3) |
| $D_J/10^{-3}$ | 5.02635(56) | 4.94599(65) | 4.9483(14) | 4.87146(46) | 5.20(1) |
| $D_{JK}/10^{-3}$ | 31.1594(35) | 30.9665(41) | 30.8208(81) | 30.6511(64) | 30.99(6) |
| $D_K/10^{-3}$ | −33.6593(66) | −33.553(45) | −33.300(68) | −33.227(14) | −33.9(1) |
| $d_1/10^{-6}$ | −24.02(50) | −37.63(62) | −42.7(12) | −50.71(17) | – |
| $d_2/10^{-6}$ | −3.302[d] | −3.302[d] | −3.302[d] | −3.302(60) | −1.4(8) |
| $H_{JK}/10^{-6}$ | −1.728[d] | −1.728[d] | −1.728[d] | −1.728(75) | – |
| $H_{KJ}/10^{-6}$ | 5.74[d] | 5.74[d] | 5.74[d] | 5.74 (35) | – |
| $\chi_{aa}$ (N1) | −2.47845(40) | – | −2.47839(87) | – | – |
| $\chi_{bb}$ (N1) | 1.24334(53) | – | 1.22864(84) | – | – |
| $\chi_{cc}$ (N1) | 1.23512(42) | – | 1.24976(81) | – | – |
| $\chi_{aa}$ (N3) | 2.18461(41) | 2.18533(43) | – | – | – |
| $\chi_{bb}$ (N3) | −3.95998(45) | −3.56374(44) | – | – | – |
| $\chi_{cc}$ (N3) | 1.77538(42) | 1.37841(42) | – | – | – |
| $\chi_{bc}$ (N3) | 0.6774(74) | 1.5977(54) | – | – | – |
| rms/kHz | 1.19 | 0.63 | 1.34 | 0.63 | 100 |
| | | | | | |
| $J$ range | 0 – 7 | 0 – 7 | 0 – 7 | 0 – 9 | 6 – 17 |
| $K_a$ range | 0 – 3 | 0 – 2 | 0 – 2 | 0 – 3 | 2 – 8 |
| # rotational transitions | 30 | 21 | 27 | 49 | 32 |
| # *b* type | 25 | 21 | 21 | 44 | –[e] |
| # *c* type | 5 | 0 | 6 | 5 | –[e] |
| # hyperfine components | 404 | 72 | 89 | 0 | [Unresolved][e] |

[a] 1σ standard deviations in the parameters are given in parentheses.
[b] Ref.[7].
[c] When calculated for this isotopologue at the B3LYP-D3BJ/aug-cc-pVTZ level, the $A_e$, $B_e$ and $C_e$ rotational constants are 4815.5 MHz, 1396.8 MHz and 1389.8 MHz respectively and the $|\mu_a|$, $|\mu_b|$ and $|\mu_c|$ dipole moments are 0.1 D, 3.6 D and 0.7 D respectively (see Table S1).
[d] Fixed at the value appropriate to Ar…imidazole-1,3-$^{15}N_2$.
[e] In this work, transitions were observed to be blended such that some *b*- and *c*-type transitions could not be distinguished from each other, preventing a determination of the number of each. Additionally, hyperfine structure was not resolved.

complexation. Three parameters are then necessary to specify the structure of Ar…imidazole: $R$ is the distance between Ar and the center of mass of imidazole, θ is the angle between the imidazole plane and $R$, and ϕ is the azimuthal angle of $R$ measured from the $a$ axis of imidazole (Fig. 5). These parameters are determined using Kisiel's STRFIT program [22] by fitting to the moments of inertia, $I_a$, $I_b$, and $I_c$, of the four isotopologues. In fact, four alternative sets of results [the results of fits (i)-(iv) as shown in Table 2 and Tables S7 – S10] can be obtained with each having low $\Delta I_{rms}$ (root mean square difference between observed and fitted moments of inertia). Fit (i) has the lowest $\Delta I_{rms}$ (0.113 u Å$^2$). The values of $\Delta I_{rms}$ for the other three sets are 1.4–2.1 times greater than this "best fit." The values of $R$ and θ in all four fits differ by no more than 0.001 Å and 0.33°, respectively. The major difference among the fits is the value of ϕ.

The values in the fits represent Ar positions in the four quadrants defined by the $a$-$b$ axis system of the imidazole monomer. The best fit gives a standard deviation of 3.9° in ϕ while the worst has a standard deviation of 9.8°. The standard deviation in ϕ thus appears rather large even for fit (i) but it is instructive to calculate the structural parameters for each isotopologue individually from its moments of inertia. For example, restricting ϕ to be acute gives the results for the four isotopologues listed at the bottom of Table 2. As expected from the small standard deviations of the values of $R$ and θ in fit (i), these parameters agree well among the isotopologues. The angle ϕ, however, has two different sets of values: 52–54° vs 60–62°. Values of ϕ are similar for different isotopologues which contain the same nitrogen isotope in the 1-position but different nitrogen isotopes in the 3-position. In the fitted geometry, N3 lies very close to the $b$ axis of the complex and isotopic substitution in this position has less effect on the results of the structure fit than does substitution at N1. In any case, the apparent large difference in the values of ϕ among the two sets of isotopologues is actually insubstantial. Within the geometrical model used, the $a/b/c$ coordinates

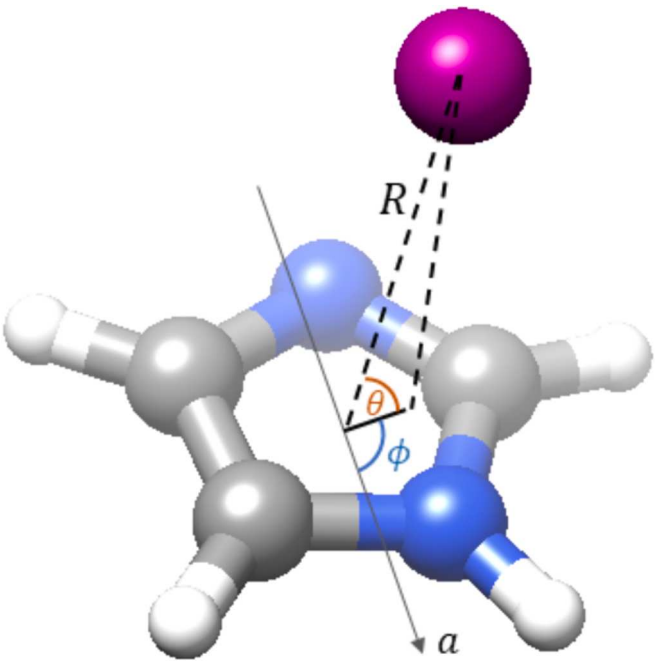


**Fig. 5.** Parameters required to characterize the structure of Ar…imidazole. $R$ is the distance between Ar and the center of mass of imidazole, θ is the elevation of Ar from the imidazole plane, and ϕ is the azimuthal angle of $R$ measured from the $a$ axis of imidazole (shown). Atom colors: C, dark gray; H, light gray, N, blue; Ar, purple.

**Table 2**
Structural parameters of Ar…imidazole determined by fits to the moments of inertia of the isotopologues and by calculating directly from each isotopologue while restricting the value of ϕ to be acute.

| | $R$/Å | θ/° | ϕ/° | $\Delta I_{rms}$[a]/u Å$^2$ |
|---|---|---|---|---|
| Fits to experimental data for all isotopologues[b] | | | | |
| Fit (i) | 3.51919 (27)[c] | 83.82 (23) | 62.0(39) | 0.113 |
| Fit (ii) | 3.51940 (36)[c] | 83.86 (32) | 120.8 (58) | 0.156 |
| Fit (iii) | 3.51853 (57)[c] | 84.15 (49) | 246.1 (98) | 0.234 |
| Fit (iv) | 3.51827 (46)[c] | 83.99 (37) | 304.6 (63) | 0.183 |
| Ref [7] | 3.516[d] | – | – | – |
| Calculation from experimental data for individual isotopologues | | | | |
| Ar…imidazole-1,3-$^{14}N_2$ | 3.51937 | 83.68 | 52.40 | |
| Ar…imidazole-1-$^{15}$N | 3.51980 | 83.54 | 61.90 | |
| Ar…imidazole-3-$^{15}$N | 3.51813 | 83.79 | 53.83 | |
| Ar…imidazole-1,3-$^{15}N_2$ | 3.51876 | 83.62 | 60.49 | |
| B3LYP-D3BJ/aug-cc-pVTZ | 3.5089[c] | 86.2 | 72.9 | |

[a] $\Delta I_{rms} = \sqrt{\sum (I_{obs} - I_{calc})^2/(\#observables - \#parameters)}$.
[b] 1σ standard deviations in the parameters are given in parentheses.
[c] The results shown imply derived point-to-plane distances of the argon atom from the plane of the imidazole ring of 3.499(62) Å, 3.499(47) Å, 3.50(16) Å and 3.498(62) Å from fits (i) – (iv) respectively. The equivalent distance from the result of the B3LYP-D3BJ/aug-cc-pVTZ calculation is 3.501 Å.
[d] The determination of $R$ made by Ref. [7] employed a variant of the Kraitchman method. See Refs. [40] and [41].

of an atom would be independent of ϕ if θ = 90° (for any given value of $R$). Given that θ ≈ 84° for the complex, the geometry is close to that limit and the 10° range in the fitted values of ϕ actually implies positions for the Ar atom that are only 0.07 Å apart. It follows that differences in the values of ϕ determined for the various isotopologues may simply reflect small changes in zero-point motions of the complex on isotopic substitution. Indeed, because the rms deviations of the four fits (Table 2) are similar and we expect the complex to exhibit large amplitude motion, it may be more appropriate to regard Ar as being located 3.519 Å from the center of mass of the imidazole monomer while undergoing large amplitude motion within a broad and shallow potential energy minimum in its zero-point state. Fig. 6 presents this potential minimum, calculated using Gaussian 16's [23] implementation of B3LYP-D3BJ/aug-cc-pVTZ. The position of the argon atom over the face of the imidazole monomer (fixed to the experimentally determined geometry of Ref. [3]) is scanned while optimizing the height of the argon atom above the imidazole plane. Indeed, the minimum is quite shallow, with the structures resulting from fits (i)–(iv) all being within 35 cm$^{-1}$ of each other. Nevertheless, fit (i) does line up very nicely with the minimum value of the potential.

The results imply that the orientations of the *a*, *b* and *c* inertial axes of the imidazole monomer (relative to the atoms of the imidazole ring) very nearly map onto the *b*, *c*, and *a* axes of the Ar…imidazole complex. For example, in the geometry determined by fit (i), an angle of only 7.4° lies between the *ab* plane of the monomer and the *bc* plane of the complex. The angle between the *ac* plane of the monomer and the *ab* plane of the complex is 9.9°; and that between the *bc* plane of the monomer and the *ac* plane of the complex is 7.9°. The rotation angles are very similar [within 2° of the result for fit (i)] for the results of fits (ii)-(iv).

The geometry determined for Ar…imidazole-1-$^{15}$N rationalizes the absence of *c* type transitions for this complex. Stark-effect measurements performed on the isolated imidazole monomer by Christen *et al.* [3] identified that the dipole moment of imidazole-1,3-$^{14}N_2$ is inclined 10.7

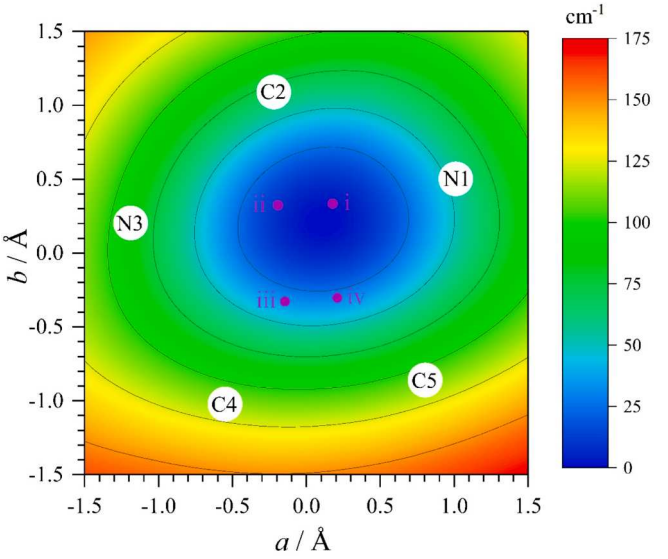


**Fig. 6.** The potential energy surface (B3LYP-D3BJ/aug-cc-pVTZ) for the argon atom moving over the face of the imidazole ring. The axes represent the location of the argon atom, with reference to the *a* and *b* inertial axis coordinates of the imidazole molecule. The distance of the argon atom above the imidazole plane is optimized to give the lowest energy. The locations of the imidazole ring atoms are indicated by white circles, and the location of the argon atom corresponding to fits (i)–(iv), described in the text, are depicted by smaller purple circles.

(5)° counter-clockwise from the *a* axis (where the rotation is about the *c* axis) of the molecule. Christen *et al.* also noted that the *a* and *b* inertial axes of imidazole-1-$^{15}$N are generated by a counter-clockwise rotation (about the *c* axis) of the inertial axis framework of the imidazole-1,3-$^{14}N_2$ parent by 10.2°. The implication is that the *a*-axis is almost parallel with the dipole moment in imidazole-1-$^{15}$N and that the dipole moment along the *b* axis of this isotopologue will therefore be extremely small. Applying the same logic to the model geometry of the Ar…imidazole complex, a counter-clockwise rotation (about the *a*-axis) of 11.2° generates the *b* and *c* inertial axes of the Ar…imidazole-1-$^{15}$N isotopologue from those of the Ar…imidazole-1,3-$^{14}N_2$ parent such that the dipole moment on the *c* axis is very small. Coupled with the fact that the number density for the complex is less than that for the monomer within the probed sample, it is unsurprising, therefore, that we do not observe *c* type transitions for Ar…imidazole-1-$^{15}$N.

### 4.3. Nuclear quadrupole coupling constants

The $\chi_{aa}$, $\chi_{bb}$ and $\chi_{cc}$, nuclear quadrupole coupling constants of a molecule are projections of its nuclear quadrupole coupling tensor onto the respective inertial axes. They can usually be determined experimentally for transitions involving low $J$ values. Rotation of the nuclear quadrupole coupling tensor from the inertial axis framework into the principal nuclear axis framework yields a diagonal matrix with $\chi_{xx}$, $\chi_{yy}$ and $\chi_{zz}$ as diagonal components which do not depend on the inertial axis orientations. It thus becomes possible to draw comparisons between $\chi_{xx}$, $\chi_{yy}$, $\chi_{zz}$, nuclear quadrupole coupling constants for nuclei within molecules and complexes even where they have widely varying geometries. The described transformation from the inertial axis framework into the principal nuclear axis framework requires that one or more of the off-diagonal components of the tensor, $\chi_{ab}$, $\chi_{bc}$ and/or $\chi_{ac}$ must be known from either experiment or theory. Experimentally-determined results are rarely available for these parameters and it has become conventional to use calculated values for this purpose. The spectroscopic fits of the present work yielded results for $\chi_{aa}$, $\chi_{bb}$ and $\chi_{cc}$ of each nucleus for all isotopologues and also for $\chi_{bc}$(N3) for the parent and Ar…imidazole-

**Table 3**
Calculated and experimentally-determined nuclear quadrupole components (in MHz) of each $^{14}$N nucleus in Ar…imidazole-1,3-$^{14}N_2$.

| | N1 | | N3 | |
|---|---|---|---|---|
| | B3LYP-D3BJ/aug-cc-pVTZ | Exp. | B3LYP-D3BJ/aug-cc-pVTZ | Exp. |
| $\chi_{aa}$ | −2.5794 | −2.47845(40) | 2.5095 | 2.18461(41) |
| $\chi_{bb}$ | 1.3163 | 1.24334(53) | −4.3652 | −3.95998(45) |
| $\chi_{cc}$ | 1.2636 | 1.23512(42) | 1.8557 | 1.77538(42) |
| $\chi_{ab}$ | 0.0992 | – | −0.0899 | – |
| $\chi_{ac}$ | 0.3629 | – | −0.0483 | – |
| $\chi_{bc}$ | 0.1408 | – | 0.5623 | 0.6774(74) |

1-$^{15}$N isotopologue. The off-diagonal components of the nuclear quadrupole coupling tensor, $\chi_{ab}$ and $\chi_{ac}$, were not determined experimentally for either N1 or N3 for any isotopologue. Calculations of the nuclear quadrupole coupling tensors were therefore performed during the present work at the B3LYP-D3BJ/aug-cc-pVTZ level to yield the results shown in Table 3. The calculated values of each ($\chi_{aa}$, $\chi_{bb}$, $\chi_{cc}$) parameter are all within 6% of the experimental results for N1 and within 15% for N3. The differences between the experimental and theoretical results reflect uncertainties in the experimental determinations which arise because of blending of transitions and the precision limits of the instrument; inaccuracies in the calculation arising from the level of theory and method employed; and because the calculation is for the $r_e$ geometry of the complex whereas the experiment is performed for the complex in the zero-point state. The agreement is only marginally improved (for some constants, and in fact worsened for others) by performing the calculation using the experimental, average structure. Such a calculation also continues to ignore the actual averaging of the parameters over the zero-point motion of the complex. We therefore assume uncertainties of 20% in the values of the DFT-calculated $\chi_{ab}$, $\chi_{bc}$ and $\chi_{ac}$ parameters used to determine $\chi_{xx}$, $\chi_{yy}$ and $\chi_{zz}$ during the present work. The signs for off-diagonal elements of the symmetric quadrupole coupling tensor depend on the arbitrary choice made for the positive direction of each Cartesian axis, although for a given choice of axis system, relative signs are significant. The signs for each nitrogen nucleus reported here are appropriate for the axis system shown for Ar…imidazole-1,3-$^{14}N_2$ in Fig. 3.

The experimentally-determined value of $\chi_{bc}$ was employed alongside the results for $\chi_{aa}$, $\chi_{bb}$ and $\chi_{cc}$ to determine $\chi_{xx}$, $\chi_{yy}$ and $\chi_{zz}$ for N3 of the Ar…imidazole-1,3-$^{14}N_2$ parent using the QDIAG program available on the PROSPE website [24]. The calculated results for $\chi_{ab}$ and $\chi_{ac}$ of this nucleus are extremely small and were included in the matrix used to perform the transformation but have negligible effects. For N1, calculated values of $\chi_{ab}$, $\chi_{bc}$ and $\chi_{ac}$ were used alongside the experimentally-determined results for $\chi_{aa}$, $\chi_{bb}$ and $\chi_{cc}$ in the transformation to determine $\chi_{xx}$, $\chi_{yy}$ and $\chi_{zz}$. In this case, the results of the transformation are more sensitive to the calculated values (and the uncertainties assumed) for each of $\chi_{ab}$, $\chi_{bc}$ and $\chi_{ac}$. The values of $\chi_{xx}$, $\chi_{yy}$ and $\chi_{zz}$ thus obtained for both nuclei, respectively, are very similar to those determined for a range of other imidazole-containing molecules and complexes [25] as shown in Table 4 and Table S11. Experimentally-determined nuclear quadrupole coupling constants depend on both the electric field gradient at the nucleus under consideration and the nature of vibrational motions within a molecule or complex. For this reason, and given the levels of uncertainties in the results, it is not possible to draw a clear correlation between the small variations in $\chi_{xx}$, $\chi_{yy}$ and $\chi_{zz}$ across the molecules and complexes featured in Table 4 and significant changes in electric field gradient at either N1 or N3 across the series. Nevertheless, the agreement between the principal nuclear quadrupole coupling constants for each nitrogen in imidazole and Ar-imidazole strongly suggest that argon perturbs the electric field gradient of imidazole minimally, if at all. Further support for this is presented below.

A useful check of internal consistency can be performed on basis of the results for $\chi_{bc}$ of the Ar…imidazole-1,3-$^{14}N_2$ and Ar…imidazole-1-$^{15}$N isotopologues. The rotation angles required to rotate the nuclear quadrupole coupling tensor of one isotopologue into the other should be consistent with the angles that transform the two respective inertial axes frameworks. In the experimental geometry of the complex [that described by the results of fit (i) in Table 2], isotopic substitution of $^{15}$N in position 1 rotates the *b* and *c* inertial axes counter-clockwise (about the *a*-axis) by 11.2° from their orientations in the parent isotopologue. The results of $\chi_{bc} = 0.6774(74)$ and 1.5977(54) MHz for Ar…imidazole-1,3-$^{14}N_2$ and Ar…imidazole-1-$^{15}$N (respectively) imply that the nuclear quadrupole coupling tensor of Ar…imidazole-1,3-$^{14}N_2$ is rotated into that of Ar-imidazole-1-$^{15}$N by a similar counter-clockwise rotation of 9.8°. The high level of consistency in these results provides a strong validation of the model geometry. It should be noted that the signs of $\chi_{bc}$ for Ar…imidazole-1,3-$^{14}N_2$ and Ar…imidazole-1-$^{15}$N are not available from experiment and depend on the arbitrary choice made for the positive directions of the *b* and *c* inertial axes. The signs chosen (and shown in Table 4) are consistent with the axes system shown in Fig. 3. In principle, if the electric field gradient at each N nucleus is unperturbed on complexation, the rotation matrix which transforms the inertial axes of the imidazole monomer into those of Ar…imidazole will be the same as that which transforms the nuclear quadrupole coupling tensor of the former into the latter. We performed this check while employing the diagonal elements of the quadrupole coupling tensor of imidazole provided by Christen *et al.* [3] and the only off-diagonal element, $\chi_{ab}$, is calculated using the same level of theory given in Section 3 (0.1485 MHz and 0.8661 MHz for the N atoms in positions 1 and 3, respectively). The diagonal components of the rotated tensors, $\chi_{aa}$, $\chi_{bb}$, and $\chi_{cc}$, differ from the experimental values for Ar…imidazole by 1.3%, 7.3%, and 4.7% for nitrogen in position 1 and by 0.3%, 0.8%, and 2.1% for nitrogen in position 3. These small differences are likely due to differences in zero-point motions in the imidazole monomer and its argon complex and uncertainties in the calculated $\chi_{ab}$ values for imidazole, and indicate that

**Table 4**
The principal nuclear quadrupole coupling components (in MHz) for imidazole and Ar…imidazole.[a]

| | Ar…imidazole | | Imidazole (Christen *et al.*[b]) | | *N*-Methylimidazole (Gougoula *et al.*[c]) | | 2-Methylimidazole (Gougoula *et al.*[c]) | |
|---|---|---|---|---|---|---|---|---|
| | N1 | N3 | N1 | N3 | N1 | N3 | N1 | N3 |
| $\chi_{xx}$ | 1.108(28) | 1.844(3) | 1.108(66) | 1.818(85) | 0.943(10) | 2.04(69) | 1.225(28) | 1.97(26) |
| $\chi_{yy}$ | 1.408(29) | 2.196(3) | 1.406(63) | 2.267(84) | 1.7427(64) | 2.1419(27) | 1.514(29) | 2.0124(59) |
| $\chi_{zz}$ | −2.516(14) | −4.040(2) | −2.514(11) | −4.085(68) | −2.6860(49) | −4.18(69) | −2.7395(58) | −3.98(27) |

[a] 1σ standard deviations in the parameters are given in parentheses.
[b] The principal nuclear quadrupole coupling components for each nitrogen are obtained using the experimental diagonal nuclear quadrupole coupling constants in Reference [3] and the $\chi_{ab}$ value computed theoretically, as given in Section 4.
[c] Reference [25]. Results for 4-methylimidazole and 5-methylimidazole (also retrieved from Reference [25]) are provided in Supplementary Table S11.

there is little, if any at all, perturbation to the electric field gradients at the nitrogen nuclei of imidazole upon complexation.

## 5. Discussion

Microwave spectroscopy has been employed to study a range of complexes formed from an aromatic molecule and an argon atom. The prototype example of Ar…benzene is a symmetric top [26]. However, the introduction of a heteroatom leads to asymmetry with respect to the position and orientation of the argon atom relative to the ring. For example, in Ar…pyrrole [27,28], Ar…pyridine [29–31], and Ar…furan [28,32–34], the distance between Ar and the center of mass of the heterocycle is always about 3.5 Å with the argon atom positioned above the ring plane but with the intermolecular axis oriented 3–11° from the normal to the heterocycle ring plane. The attractive interaction between argon and an electronegative heteroatom such as oxygen or nitrogen leads to the described asymmetry. The deviation of the intermolecular axis from the normal is greater for Ar…furan than for Ar…pyridine [29] or Ar…pyrrole [27], probably because oxygen is smaller and more electronegative than nitrogen.

The structures of complexes formed between Ar and heterocycles such as pyrazole, pyridazine and pyrimidine (which each contain two heteroatoms) are also known. In every case, the distance from the Ar atom to the center of mass of the heteroaromatic ring is about 3.5 Å. In Ar…pyrazole, the intermolecular axis forms an angle of 8° with the normal to the ring plane and this axis is rotated 13° with respect to the N-H orientation [35]. Experiments performed to study Ar…pyridazine [36] and Ar…pyrimidine [37] established that the intermolecular axis deviates from the normal to the plane within each complex. However, they did not unambiguously define the position and orientation of the argon atom relative to the heterocyclic ring, having been performed only for a single isotopologue of each complex. In each of Ar…pyridazine and Ar…pyrimidine, therefore, it is presumed that the Ar is closer to the nitrogens than to other atoms within the ring. Microwave spectroscopy and *ab initio* calculations performed for the Ar…oxazole complex confirm that Ar is closer to oxygen than to the other atoms in the heterocycle with the intermolecular axis oriented 9° from the normal to the ring plane [38].

The results of the present work have been achieved through analysis of the spectra recorded for four isotopologues. The data set thus allows for high precision in the determination of two structural parameters ($R$, $\theta$) even while there remains ambiguity in a third ($\phi$). The distance between Ar and the center of mass of imidazole ($R$) is 3.519 Å and the intermolecular axis is oriented 6° from the normal (determined as 90° – $\theta$) to the imidazole plane. The result for $R$ is very similar to that of 3.516 Å reported earlier which justifies the approximation, based on the Kraitchman method [39] (see also Refs. [40;41]), used by Caminati *et al.* [7] and reflects that this parameter is minimally sensitive to the values of $\theta$ and $\phi$. Ambiguity in $\phi$ exists because of the high degree of symmetry in the distribution of mass with respect to rotation of the ring about the normal to the ring plane within the complex. As might be expected, therefore, the four solutions for the molecular geometry as identified in Table 2 [fits (i)-(iv)] can be interchanged by a 90° rotation of the ring about the normal to the plane followed by a small movement of the argon atom. Moreover, as noted earlier, the four solutions may largely reflect small differences in zero-point vibrational motions on isotopic substitution. The lowest residuals are achieved for those two sets of results which are most consistent with the results of previous works to study other complexes, and also with the result of the B3LYP-D3BJ/aug-cc-pVTZ calculation performed during the present work. Specifically, the solutions where $\phi$ is either 62.0(39)° or 120.8(58)° would place the argon atom on that side of the imidazole ring which is closest to the nitrogen atoms as would be expected from consideration of the electronegativities of the atoms within the ring. The result of 62.0(39)° is closest to that of 72.9° yielded by the B3LYP-D3BJ/aug-cc-pVTZ calculation. Given the relatively weak intermolecular interaction between argon and imidazole, large amplitude motions are to be expected that will cause the instantaneous geometry of the complex to deviate significantly from that determined through the present analysis, which employs the assumption of a semi-rigid geometry for the molecule in its ground vibrational state. Nevertheless, it is satisfying to note the high level of agreement between the values of $R$ and $\theta$ determined herein for Ar…imidazole and those reported previously for similar complexes.

## 6. Conclusions

Measurement of pure rotational spectra for four isotopologues of the imidazole…Ar complex has allowed three intermolecular parameters in the structure of the complex to be determined from rotational constants fitted to the observed transition frequencies. The angles which define the orientation of the argon atom relative to the imidazole ring have been determined for the first time. The orientation of the intermolecular axis (defined by a line which passes through argon and the center of mass of imidazole) tilts slightly ($90° - \theta \cong 6°$) away from the normal of the imidazole plane. The experimental results allow various possibilities for $\phi$, the angle between the projection of the internuclear axis onto the plane of the ring and the $a$ axis of the imidazole monomer sub-unit. A result of $\phi = 62.0(39)°$ is most consistent with the result of a B3LYP-D3BJ/aug-cc-pVTZ calculation and with expectations based on previous work which suggest that an attractive interaction will draw the argon atom toward the nitrogen atoms of the ring. The experimentally-determined nuclear quadrupole coupling constants show that the attachment of argon to imidazole does not lead to significant perturbation of the electric field gradient within the heteroaromatic ring.

## CRediT authorship contribution statement

**Ryan Welch:** Writing – review & editing, Writing – original draft, Visualization, Methodology, Investigation, Formal analysis, Data curation. **Mark D. Marshall:** Writing – review & editing, Validation, Supervision, Resources, Project administration, Methodology, Funding acquisition, Formal analysis, Data curation. **Eva Gougoula:** Writing – review & editing, Visualization, Validation, Investigation. **Nicholas R. Walker:** Writing – review & editing, Validation, Resources, Methodology, Formal analysis, Data curation. **Helen O. Leung:** Conceptualization, Methodology, Validation, Formal analysis, Investigation, Resources, Data curation, Writing – original draft, Writing – review & editing, Visualization, Supervision, Project administration, Funding acquisition.

## Declaration of competing interest

The authors declare that they have no known competing financial interests or personal relationships that could have appeared to influence the work reported in this paper.

## Data availability

Data will be made available on request.

## Acknowledgments

We thank Dr. Richard Suenram for his advice on the construction of a heated nozzle. This material is based on work supported by the National Science Foundation under Grant No. CHE-2309942. We thank Newcastle University for a research studentship (for E.G.) and the European Research Council for project funding (Grant No. CPFTMW-307000).

## Appendix A. Supplementary data

Supplementary data to this article can be found online at https://doi.org/10.1016/j.jms.2024.111948.

## References


[1] T.L. Gilchrist, Heterocyclic Chemistry, 2nd ed., John Wiley & Sons, New York, 1992.

[2] E. Gougoula, C.N. Cummings, C. Medcraft, J. Heitkämper, N.R. Walker, Microwave spectra, molecular geometries, and internal rotation of $CH_3$ in *N*-methylimidazole···$H_2O$ and 2-methylimidazole···$H_2O$ complexes, Phys. Chem. Chem. Phys. 24 (2022) 12354–12362.

[3] D. Christen, J. Griffiths, J. Sheridan, The microwave spectrum of imidazole; complete structure and the electron distribution from nuclear quadrupole coupling tensors and dipole moment orientations, Z.Naturforsch. 36a (1982) 1378-1385.

[4] J.H. Griffiths, A. Wardley, V.E. Williams, N.L. Owen, J. Sheridan, Microwave spectra and structures of isothiazole, 1,2,4-oxadiazole and imidazole, Nature 216 (1967) 1301.

[5] G.L. Blackman, R.D. Brown, F.R. Burden, I.R. Elsum, Nuclear quadrupolar coupling in the microwave spectrum of imidazole, J. Mol. Spectrosc. 60 (1976) 63–70.

[6] B.M. Giuliano, L. Bizzocchi, A. Pietropolli Charmet, B.E. Arenas, A.L. Steber, M. Schnell, P. Caselli, B.J. Harris, B.H. Pate, J.C. Guillemin, A. Belloche, Rotational spectroscopy of imidazole: improved rest frequencies for astrophysical searches, Astron.Astrophys. 628 (2019) A53.

[7] W. Caminati, S. Melandri, A. Millemaggi, P.G. Favero, Rotational spectrum of the imidazole-argon complex, Chem. Phys. Lett. 294 (1998) 377–380.

[8] H.O. Leung, D. Gangwani, J.U. Grabow, Nuclear quadrupole hyperfine structure in the microwave spectrum of Ar-$N_2O$, J. Mol. Spectrosc. 184 (1997) 106–112.

[9] S.L. Stephens, N.R. Walker, Determination of nuclear spin–rotation coupling constants in $CF_3I$ by chirped-pulse Fourier-transform microwave spectroscopy, J. Mol. Spectrosc. 263 (2010) 27–33.

[10] D.P. Zaleski, S.L. Stephens, N.R. Walker, A perspective on chemistry in transient plasma from broadband rotational spectroscopy, Phys. Chem. Chem. Phys. 16 (2014) 25221–25228.

[11] R.D. Suenram, G.Y. Golubiatnikov, I.I. Leonov, J.T. Hougen, J. Ortigoso, I. Kleiner, G.T. Fraser, Reinvestigation of the microwave spectrum of acetamide, J. Mol. Spectrosc. 208 (2001) 188–193.

[12] S.L. Stephens, W. Mizukami, D.P. Tew, N.R. Walker, A.C. Legon, Molecular geometry of OC•••AgI determined by broadband rotational spectroscopy and *ab initio* calculations, J. Chem. Phys. 136 (2012) 064306.

[13] F. Neese, Software update: The ORCA program system—version 5.0, WIREs Comput. Mol. Sci. 12 (2022) e1606.

[14] F. Neese, F. Wennmohs, U. Becker, C. Riplinger, The ORCA quantum chemistry package, J. Chem. Phys. 152 (2020) 224108.

[15] A.D. Becke, Density-functional thermochemistry. III. The role of exact exchange, J. Chem. Phys. 98 (1993) 5648-5652.

[16] B. Miehlich, A. Savin, H. Stoll, H. Preuss, Results obtained with the correlation energy density functionals of Becke and Lee, Yang and Parr, Chem. Phys. Lett. 157 (1989) 200–206.

[17] S. Grimme, J. Antony, S. Ehrlich, H. Krieg, A consistent and accurate ab initio parametrization of density functional dispersion correction (DFT-D) for the 94 elements H-Pu, J. Chem. Phys. 132 (2010) 154104.

[18] S. Grimme, S. Ehrlich, L. Goerigk, Effect of the damping function in dispersion corrected density functional theory, J. Comput. Chem. 32 (2011) 1456–1465.

[19] R.A. Kendall, T.H. Dunning, Jr., R.J. Harrison, Electron affinities of the first-row atoms revisited. Systematic basis sets and wave functions, J. Chem. Phys. 96 (1992) 6796-6806.

[20] J.K.G. Watson, Aspects of quartic and sextic centrifugal effects on rotational energy levels, in: J.R. Durig (Ed.), Vibrational Spectra and Structure, Elsevier Scientific Publishing, Amsterdam, 1977, pp. 1–89.

[21] H.M. Pickett, The fitting and prediction of vibration-rotation spectra with spin interactions, J. Mol. Spectrosc. 148 (1991) 371–377.

[22] Z. Kisiel, Least-squares mass-dependence molecular structures for selected weakly bound intermolecular clusters, J. Mol. Spectrosc. 218 (2003) 58–67.

[23] M.J. Frisch, G.W. Trucks, H.B. Schlegel, G.E. Scuseria, M.A. Robb, J.R. Cheeseman, G. Scalmani, V. Barone, G.A. Petersson, H. Nakatsuji, X. Li, M. Caricato, A.V. Marenich, J. Bloino, B.G. Janesko, R. Gomperts, B. Mennucci, H.P. Hratchian, J.V. Ortiz, A.F. Izmaylov, J.L. Sonnenberg, F. Williams-Young, F. Ding, F. Lipparini, F. Egidi, J. Goings, B. Peng, A. Petrone, T. Henderson, D. Ranasinghe, V.G. Zakrzewski, J. Gao, N. Rega, G. Zheng, W. Liang, M. Hada, M. Ehara, K. Toyota, R. Fukuda, J. Hasegawa, M. Ishida, T. Nakajima, Y. Honda, O. Kitao, H. Nakai, T. Vreven, K. Throssell, J.A. Montgomery Jr., J.E. Peralta, F. Ogliaro, M.J. Bearpark, J.J. Heyd, E.N. Brothers, K.N. Kudin, V.N. Staroverov, T.A. Keith, R. Kobayashi, J. Normand, K. Raghavachari, A.P. Rendell, J.C. Burant, S.S. Iyengar, J. Tomasi, M. Cossi, J.M. Millam, M. Klene, C. Adamo, R. Cammi, J.W. Ochterski, R.L. Martin, K. Morokuma, O. Farkas, J.B. Foresman, D.J. Fox *Gaussian 16*, Revision A.03; Gaussian, Inc.: Wallingford, CT, 2016.

[24] Z. Kisiel PROSPE - Programs for ROtational SPEctroscopy. http://info.ifpan.edu.pl/~kisiel/prospe.htm (accessed May 21, 2024).

[25] E. Gougoula, C. Medcraft, J. Heitkämper, N.R. Walker, Barriers to internal rotation in methylimidazole isomers determined by rotational spectroscopy, J. Chem. Phys. 151 (2019) 144301.

[26] T. Brupbacher, A. Bauder, Rotational spectrum and dipole moment of the benzene-argon van der Waals complex, Chem. Phys. Lett. 173 (1990) 435.

[27] R.K. Bohn, K.W. Hillig II, R.L. Kuczkowski, Pyrrole-argon: microwave spectrum, structure, dipole moment, and nitrogen-14 quadrupole coupling constants, J. Phys. Chem. 93 (1989) 3456–3459.

[28] J.J. Oh, K.W. Hillig II, R.L. Kuczkowski, R.K. Bohn, Dipole moments of furan-argon and pyrrole-argon, J. Phys. Chem. 94 (1990) 4453–4455.

[29] T.D. Klots, T. Emilsson, R.S. Ruoff, H.S. Gutowsky, Microwave spectra of noble gas-pyridine dimers: Argon-pyridine and krypton-pyridine, J. Phys. Chem. 93 (1989) 1255–1261.

[30] R.M. Spycher, D. Petitprez, F.L. Bettens, A. Bauder, Rotational spectra of pyridine-$(argon)_n$, $n = 1, 2$, complexes and their vibrationally averaged structures, J. Phys. Chem. 98 (1994) 11863–11869.

[31] S. Melandri, G. Maccaferri, A. Maris, A. Millemaggi, W. Caminati, P.G. Favero, Observation of the rotational spectra of van der Waals complexes by free jet absorption millimeter wave spectroscopy: Pyridine- argon, Chem. Phys. Lett. 261 (1996) 267–271.

[32] S.G. Kukolich, J.A. Shea, The microwave spectrum and molecular structure of the furan–argon complex, J. Chem. Phys. 77 (1982) 5242–5243.

[33] S.G. Kukolich, Microwave structure measurements on the furan-argon complex, J. Am. Chem. Soc. 105 (1983) 2207–2210.

[34] R.M. Spycher, L. Hausherr-Primo, G. Grassi, A. Bauder, Rotational spectra of isotopic furan-$(argon)_n$, $n = 1,2$, complexes and their vibrationally averaged structures, J. Mol. Struct. 351 (1995) 7–17.

[35] W. Caminati, P.G. Favero, B. Velino, Adducts of aromatic molecules with rare gases: rotational spectrum of pyrazole–argon, Chem. Phys. 239 (1998) 223–227.

[36] W. Caminati, A. Millemaggi, P.G. Favero, J. Makarewicz, Free jet absorption millimeter wave spectrum and van der Waals potential energy surface of the pyridazine-argon adduct, J. Phys. Chem. A 101 (1997) 9272–9275.

[37] W. Caminati, P.G. Favero, S. Melandri, R. Meyer, Free jet absorption millimeter wave spectrum of the pyrimidine-argon molecular complex, Chem. Phys. Lett. 268 (1997) 393–400.

[38] E. Kraka, D. Cremer, U. Spoerel, I. Merke, W. Stahl, H. Dreizler, Intermolecular forces in argon van der Waals complexes. Rotational spectrum and ab initio investigation of Ar- oxazole, J. Phys. Chem. 99 (1995) 12466-12477.

[39] J. Kraitchman, Determination of molecular structure from microwave spectroscopic data, Am. J. Phys. 21 (1953) 17–24.

[40] E. Jochims, J.U. Grabow, W. Stahl, Microwave spectrum and structure of the 1,2-difluorobenzene argon van der Waals complex, J. Mol. Spectrosc. 158 (1993) 278–286.

[41] M.R. Munrow, W.C. Pringle, S.E. Novick, Determination of the structure of the argon cyclobutanone van der Waals complex, J. Phys. Chem. A 103 (1999) 2256–2261.